Laser and Particle Beams (2001), *19*, 527–540. Printed in the USA.

DOI: 10.1017.S0263034600194029

The magneto-Rayleigh–Taylor instability in dynamic *z* pinches

M.R. DOUGLAS, J.S. DE GROOT, AND R.B. SPIELMAN
Sandia National Laboratories, Albuquerque, NM 87185-1194, USA

(RECEIVED 22 May 2000; ACCEPTED 20 April 2001)

Abstract

The magneto-Rayleigh–Taylor (MRT) instability limits the performance of dynamic *z* pinches. This instability develops at the plasma-vacuum/field interface, growing in amplitude throughout the implosion, thereby reducing the peak plasma velocity and spatial uniformity at stagnation. MRT instabilities are believed to play a dominant role in the case of high wire number arrays, gas puffs and foils. In this article, the MRT instability is discussed in terms of initial seeding, linear and nonlinear growth, experimental evidence, radiation magnetohydrodynamic simulations, and mitigating schemes. A number of experimental results are presented, where the mitigating schemes have been realized. In general, the problem is inherently three dimensional, but two-dimensional simulations together with theory and experiment enhance our physical understanding and provide insight into future load design.

1. INTRODUCTION

World-record laboratory X-ray power and radiated energy have been obtained with tungsten wire array loads (Deeney *et al*., 1998) that are imploded by a fast *z* pinch. Specifically, X-ray powers of over 250 TW (Deeney *et al*., 1998) have been measured on the Z 50-TW accelerator (Spielman *et al*., 1998) at Sandia National Laboratories in Albuquerque, NM. These results have generated a renaissance in *z*-pinch research. Even with such high radiated powers and energies, it is believed that the performance of the *z* pinch may be limited by the magneto-Rayleigh–Taylor (MRT) instability (Liberman *et al*., 1999, Chapter 5). This instability has been experimentally observed in gas puffs in highly resolved pinhole-camera images (Douglas *et al*., 1997; Levine *et al*., 2001), in foils using visible light framing cameras (Peterson *et al*., 1996), and has been inferred from high wire number array data. The MRT instability is similar to the classical Rayleigh–Taylor (R-T) instability in which a light fluid supports a heavy fluid against gravity. Plasma is imploded (accelerated) in a dynamic pinch by the pressure due to the azimuthal magnetic field. Thus, the plasma, in its own frame of reference, represents a "heavy fluid," which is supported by a "massless fluid" (i.e., by the magnetic field) in a gravitational field; this configuration exhibits the R-T instability. In this respect, *z* pinches are quite similar to other systems in which plasma or solid objects are electromagnetically accelerated. Such examples include rail guns and other electromagnetic guns, and also laser fusion systems of plasma acceleration, where the high-temperature, low-density, plasma corona acts as a "light fluid" (Lindl, 1995). To assess the importance of any instability, both the initial amplitude of the unstable modes and the growth rate of these modes must be determined. In a dynamic *z* pinch, the plasma is accelerated in the radial direction, so the fastest MRT mode grows from density (and/or fluid velocity) perturbations that depend on the axial coordinate, that is, $\rho(z)$.

Address correspondence and reprint requests to: M.R. Douglas, P.O. Box 5800, Sandia National Laboratories, Albuquerque, NM 87112, USA. E-mail: mrdougl@sandia.gov

2. MRT FUNDAMENTALS

2.1. Initial perturbations

An instability grows in a fluid from initial perturbations in velocity, displacement, and/or density. In a gas-puff *z* pinch, these perturbations are believed to be due to axial and radial density gradients formed from the expansion of the supersonic gas flow out of a nozzle. In a wire array, these perturbations could be due to either sausage and/or kink instabilities of the individual wire plasmas, wire–wire interactions, or nonuniform plasma formed in the wire–plasma initiation process. In the latter case, variations in wire location, nonuniform plasma formed by wire breakdown, nonuniform wire composition, and low atomic number impurities (primarily hydrogen and carbon) on the wire surface could lead to such a plasma distribution. Recent improvements in

experimental diagnostics have provided a means to accurately measure the mass distribution in gas puffs (Song *et al*., 2000). This is useful in defining the seed for the instability growth in corresponding simulations. For wire arrays, this capability has not yet been fully realized. X-ray imaging, laser interferometry, and Schlieren techniques on low wire number arrays have provided some impressive measurements of the plasma distribution and evolution prior to array acceleration (Lebedev *et al*., 1999, 2000). However, the plasma distribution in a wire array tends to be quite complex, defined not only by the wire material, but the number of wires, and the temporal-shape of the current pulse driving the system. Experimental data confirms this, suggesting that there are different regimes of wire array implosions based on the initial array configuration and composition (Deeney *et al*., 1999). This will be discussed in more detail in Section 3.

2.2. MRT instability growth

A *z*-pinch implosion is time dependent, so the usual normal mode analysis in which the unperturbed quantities are time independent cannot be used to determine mode growth. However, if the time evolution is slow enough compared to the instantaneous growth rate, that is, if τ is the characteristic time constant of the implosion and Γ is the instantaneous growth rate, then $\tau\Gamma \gg 1$, and the time dependence of the perturbations, $F(t)$, is well approximated by a Wentzel–Kramer–Brillouin (WKB) integral:

$$F(t) = \exp\left[\int_0^{-t} \Gamma(t')dt\right] \equiv \exp\{n_{eff}(t)\}. \quad (1)$$

Here $\Gamma(t)$ is the instantaneous growth rate of the corresponding instability mode, which is calculated by using the unperturbed quantities at time *t*. The fastest growing MRT small amplitude mode has a growth rate (Liberman *et al*., 1999, Section 5.1) given by

$$\Gamma \approx (ka)^{1/2},$$

where k is the axial wave number and a is the acceleration. If the amplitude of the unstable mode, δ, is larger than $1/k$, that is, $\delta k > 1$, then the instability growth rate is reduced (Liberman *et al*., 1999, Section 5.7).

The mathematical prescription of mode growth, as characterized by Eq. (1), is a useful approximation when considering MRT development. However, nonlinear mode growth combined with nonlinear mode coupling further complicates this simple prescription. Nonetheless, a conservative estimate for the total number of e-foldings can be obtained by taking Eq. (1) for the growth rate and assuming the acceleration to be constant during the implosion. Then the total number of e-foldings is $n_{eff} = (2kr_0)^{1/2}$, where r_0 is the initial radius of the plasma. Since the experimentally observed wavelengths are in the range of $\lambda \sim 0.1$ cm (Deeney *et al*., 1997*a*; Sanford *et al*., 1997*a*), $n_{eff} \sim 15$ for a typical plasma shell with a 40-mm initial diameter. Since the number of e-foldings is very large, that is, $n_{eff} \gg 1$, the MRT unstable modes grow to large amplitude during a typical *z*-pinch implosion.

2.3. Structure of the nonlinear modes

In the linear phase of the MRT instability development, when the initial perturbations are small compared to the wavelength, the small amplitude perturbations grow exponentially in time. This early stage in the growth of the instability can be analyzed using the linearized form of the dynamical equations for the plasma. In the nonlinear phase of the instability, where the amplitude of the initial perturbations grow to a value of order $1/k$, the perturbations may grow slower than exponential (depending on plasma conditions) and the familiar spike and bubble structure is formed. The final phase of growth is characterized by the development of structure on the spikes and interaction among the bubbles; further growth implies ejection of a significant fraction of mass from the bubble region to the spike. This can continue until the mass per unit area of the bubble becomes very small. There are several complicating features of this phenomenon (see Liberman *et al*., 1999). The most significant features are nonlinear interaction among initial perturbations of different frequencies (mentioned in the above section), and bubble amalgamation, when larger bubbles absorb smaller ones, with the result that the larger bubbles grow even larger and move faster.

There is considerable literature on the nonlinear evolution of the R-T instability (for instance, see Chandrasekhar, 1961; the reviews by Sharp, 1984; Kull, 1991; and references therein). Experimental and computational evidence suggests that full three-dimensional (3-D) simulations are required to accurately calculate the nonlinear R-T instability evolution (Manheimer *et al*., 1984; Orszag, 1984; Sakagami & Nishihara, 1990; Town & Bell, 1991; Dahlburg *et al*., 1993; Dunning & Haan, 1995). The MRT instability is less understood and has many features that do not occur in R-T instabilities. For example, the plasma typically represents a medium of finite thickness, and thus bubbles can eventually burst through into the inner vacuum region (Hussey *et al*., 1995). When this occurs, magnetic flux may be carried into the central vacuum by a very low-density plasma ahead of the bulk of the plasma mass, decreasing the effective acceleration of the pinch (for simulated evidence of reduction in effective acceleration, see Douglas *et al*., 2001). The magnetic field also diffuses into the resistive plasma. This spreads the acceleration over a distance characterized by the magnetic diffusion scale length, and can slow the growth rate of the MRT instability (Hammer *et al*., 1996). For an introduction to and historical perspective on MRT in *z*-pinch implosions, including nonlinear development, refer to the papers of Roderick, Hussey, and Kloc (Hussey *et al*., 1980, 1986; Roderick *et al*., 1980, 1986; Hussey & Roderick, 1981; Kloc

https://doi.org/10.1017/S0263034600194029 Published online by Cambridge University Press

et al., 1982; Roderick & Hussey, 1984). Such papers represent the original seminal work in this field, providing the foundation for later MRT investigations.

As mentioned, many *z*-pinch configurations consist of a finite thickness plasma, that is, a wire array or annular gas puff. Thus, the stability of thin shells that are accelerated by the pressure of a low-density fluid, or thin shells that are accelerated radially inward, is of special importance in these cases. Both two-dimensional (2-D) simulations (i.e., Peterson *et al*., 1996) and phenomenological modeling of the nonlinear MRT phase (Hussey *et al*., 1995) indicate that the most damaging modes for thin-shelled systems are those with wavelengths that are on the order of, or a few times larger than, the initial shell thickness. This means that a thin-layer approximation, where a fluid layer is approximated as an infinitely thin sheet with a finite surface density, can be useful in investigating such instabilities. Two dimensional simulations for an incompressible, nonmagnetized fluid (Manheimer *et al*., 1984) have shown that the thin layer approximation is reasonably good, not only in the limit $\lambda \gg d$ (shell thickness), but even for wavelengths as small as $\lambda = 2\pi d$.

The flow pattern in the nonlinear stage of R-T is determined to a large extent by the nonlinear interaction of perturbations with different wavelengths, λ, and by energy transfer from small-scale to large-scale perturbations. Though the nonlinear evolution of a perturbation with a fixed wavelength has been studied in detail, the picture of the development of initially chaotic perturbations is not yet clear. Even though most qualitative features of a 2-D flow remain unchanged, such as the bubbles of the light fluid rising up and the spikes of the heavy fluid falling down, many important issues require further study. In particular, it is not yet known whether the size and velocity distributions of the bubbles tend to universal functions or depend on the initial conditions. In addition, even when the flute, purely interchange-perturbation modes are studied, for which a magnetic field acts to support or accelerate the plasma and behaves in an ideal MHD model as a massless fluid, the nonlinear evolution may be affected by some factors specific to electromagnetic acceleration and beyond ideal MHD.

3. *Z*-PINCH EXPERIMENTS AND MRT SIMULATIONS

Z-pinch implosions are fundamentally complex. To study the effect of MRT development on pinch performance requires not only an understanding of MRT growth throughout the implosion, but also of the initiation phase of the load prior to acceleration. This latter process, in conjunction with the plasma distribution, is believed to form the seed for the MRT instability. Out of the standard loads that have been used as *z* pinches, that is, gas puffs (Spielman *et al*., 1985; Deeney *et al*., 1993), foils (Matuska *et al*., 1996), wire arrays (Giuliani *et al*., 1990; Sanford *et al*., 1996; Deeney *et al*., 1997*a*,*b*), and foams (Derzon *et al*., 1997), wire arrays are probably the most widely used yet difficult to model. Clearly, wire arrays are three dimensional in nature and the physical process of initiation and consequent implosion are not well diagnosed for many cases. This is particularly true for ultrafast (40 cm/μs to 130 cm/μs) implosions (Deeney *et al*., 1997*a*) driven by multi-MA drivers (Spielman *et al*., 1989, 1998). Innovative diagnostics, such as the *X*-pinch backlighter (Shelkovenko *et al*., 1999), and improvements in existing diagnostics, that is, high-resolution pinhole cameras and Schlieren techniques, have enabled a detailed study of wire explosions and the implosion dynamics of low wire number arrays on small pulsed-power machines ($<$1 MA). In particular, individual wire and double wire experiments have been carried out at Cornell University (Pikuz *et al*., 1999*a*, 1999*b*; Sinars *et al*., 2000, 2001), Imperial College (Figura *et al*., 1991; Beg *et al*., 1997; Ruiz-Camacho *et al*., 1999), and the University of Nevada, Reno (Sarkisov *et al*., 2001) using a variety of materials with current depositions ranging from 0.1 kA/ns to 1 kA/ns. Such experiments have been modeled extensively in two dimensions by Reisman (2001), Chittenden *et al*. (1997, 2000), and Desjarlais *et al*. (1999*b*) using magnetohydrodynamic (MHD) codes.

Low number wire arrays ranging from 8 to 64 wires have been imploded with the MAGPIE generator (Mitchell *et al*., 1996) at Imperial College (Lebedev *et al*., 1998, 1999, 2000), where the most extensive work has focused on Al as the wire material. These experiments illustrate that there are many details of wire plasma initiation and implosion dynamics that occur with low wire number (i.e., large interwire-gap spacing), low-current drives. Such details can alter the initial mechanism for MRT seeding and influence the subsequent MRT development as the bulk of the array implodes. The most important features of these implosions include the observation of precursor material streaming towards the stagnation axis and a global MRT-like structure of hot spots (along individual wires) observed in X-ray pinhole camera images of the wire array prior to the main implosion. The amount and distribution of precursor material appears to be dependent upon the wire composition and the number, with an appreciable decrease in precursor with increasing wire number. The MRT-like structure that has been observed may be correlated to individual wire instabilities that develop in the expanding wire corona, and the balance between private and global magnetic fields. Haines (1998) has developed a heuristic model based on such an explanation.

Although, there appears to be evidence of MRT seeding, the MAGPIE arrays do not typically implode as shell-like loads that are accompanied by an MRT instability. At this time, it is not well known how these dynamics scale to larger current machines which generally have much higher wire numbers ($>$180) and smaller interwire-gap spacings. Interestingly enough, the Haines heuristic model can predict pulse widths of high wire number arrays on the Z accelerator (Deeney *et al*., 1999; Sanford *et al*., 1999), but cannot sufficiently account for the results obtained with low wire

https://doi.org/10.1017/S0263034600194029 Published online by Cambridge University Press

number arrays. However, the model can predict where the transition between high wire and low wire number arrays might occur.

Conventional modeling of gas puffs (Hammer *et al*., 1996; Douglas *et al*., 1997), foils (Bowers *et al*., 1996), and high wire number (Peterson *et al*., 1997; Sanford *et al*., 1998; Deeney *et al*., 1999; Douglas *et al*., 2000*b*) pinches has mostly been done with two-dimensional MHD codes in the *r*–*z* plane. Here, the pinch is approximated by a right cylindrical shell (or uniform cylinder if modeling a uniform-fill gas puff or foam) with a random perturbation in either density or velocity to seed the MRT instability. Such calculations have been quite successful in modeling the radiated properties at stagnation, as well as the overall structure of the pinch prior to stagnation as observed with X-ray pinhole camera images. In this approach, the initial perturbation level is varied to obtain the best comparison between the measured and simulated results. This suggests that three-dimensional effects, which are most obvious in the context of wire arrays, may only add an additional perturbation to the simulated approximation in particular cases. (The details of 2-D *r*–*z* simulations will be described later in this paper.)

For low wire number arrays, an analytic approach is usually taken. Desjarlais and Marder (1999*a*) have proposed that 3-D effects that occur in low wire number cases may be based on a kink-amplified MRT behavior. Here, an increased growth beyond that predicted in two-dimensional simulations results from kink-like forces on individual wires. This model can be used to estimate pulse widths (an initial wavelength and amplitude must be defined) and has had some success in matching to experimental data. A complete classification of linear instability modes in a wire array using a thin wire approximation has been carried out by Hammer and Ryutov (1999). Their results provide a means to evaluate the growth rate of any linear mode and is particularly useful in the low wire number regime where MHD modeling is difficult. To date, many of the low wire-number MAGPIE results involving precursor development and flow have not yet been numerically simulated. However, a small number of these wire array experiments have been modeled on some level by Chittenden in both two and three dimensions (Chittenden *et al*., 1999, 2001).

As mentioned, the experimental data on single wire initiation and low wire number, low current wire array implosions can provide information on the physical processes that define the later stages of implosion dynamics and stagnation. Modeling these experiments is important in that it benchmarks the state-of-the-art MHD codes used to simulate *z*-pinch implosions. In doing this, the limitations of the simulation based on physical models and approximations incorporated in the codes can be determined. Single wire initiation calculations are useful in that the computationalist can gain understanding of the physical process of wire initiation and how it influences core-corona development and single wire instabilities. The knowledge and experience gained in modeling such experiments can then be extended to model an array of wires. Clearly, data from the MAGPIE experiments suggest that the physics involved in single wire explosions can be strongly modified by the introduction of a wire array configuration and cannot ultimately produce an integrated picture of the wire array dynamics from initiation through implosion. Nonetheless, such simulations provide a first step towards physical understanding. Improvements in electrical resistivity models have been introduced independently by Reisman (2001), Desjarlais (2001), and Rosenthal *et al*. (2000). In the latter case, the resistivities result from a new ionization equilibrium model and modifications to the Lee–More algorithm in order to accurately characterize the metal-insulator transition regime. The resulting simulations have accurately modeled many of the measurable quantities such as voltage and corona expansion to within experimental error bars.

Recent work on the Saturn machine at Sandia National Laboratories has further elucidated the physical regimes that may occur between low and increasingly high wire number array implosions (Deeney *et al*., 1999; Douglas *et al*., 2000*a*). A comparison of tungsten wire arrays imploded in both a short- and long-pulse mode show that an improvement in X-ray production was observed in the long-pulse mode, even though the diameters of these arrays were a factor of two larger and had lower implosion velocities than their short-pulse counterparts. (In the short-pulse mode, Saturn can deliver a peak current of approximately 8 MA to a wire array load in 100 ns, while in the long-pulse mode, the machine can deliver 8 MA in 130 ns to a short circuit. With additional mass loading, the implosion time could be varied up to 240 ns.) This improvement has been examined using the conventional simulation approach of 2-D *r*–*z* radiation MHD modeling (Douglas *et al*., 2000*a*). The calculations show that a cell-to-cell random density perturbation (used to seed the instability) throughout an initially 1-mm-thick shell could not reproduce the short pulse data up to a perturbation level of 40%. On the other hand, the long implosion-time data could be matched with an initial perturbation level ranging between 1% and 5%. These computational results, when combined with a heuristic model (Haines, 1998) of wire initiation and merger, could explain the long-pulse improvements in radiated quantities; the long-implosion-time results observed were a consequence of improved initial conditions for the implosions. With merger loosely defined to occur when adjacent wire coronas reach half the interwire-gap spacing, the individual wires comprising the long-pulse array had more time, that is, between 60 and 100 ns to heat and expand before being accelerated. This gave the wire plasma a longer time to develop and merge with nearby wires, compared to 25 ns in the short-pulse mode, thus forming a more uniform mass distribution, or shell, prior to acceleration. Furthermore, coronal merging acts as a Faraday cage, reducing plasma precursor and smoothing out the magnetic pressure drive. Such a configuration is amenable to the standard methodology used in 2-D *r*–*z* simulations.

https://doi.org/10.1017/S0263034600194029 Published online by Cambridge University Press

The results of the Saturn tungsten study suggest that wire merger may determine whether a pinch implodes with a 2-D shell-like nature with an implosion phase dominated by MRT growth, or as a complex 3-D entity. To further investigate this, an Al wire-number scan was subsequently carried out in the Saturn long-pulse mode (Deeney *et al*., 2000; Douglas *et al*., 2000*c*), to see if a transition, based on wire number and merger, could be observed. In this experimental campaign, the wire-array mass and diameter was fixed, and only the wire number (and, hence, interwire-gap spacing) was varied. The wire number ranged from 32 to 282 wires, corresponding to a gap spacing from 3.9 mm to 0.4 mm. For a constant current drive, merger is prescribed by the wire expansion velocity and interwire-gap spacing (i.e., wire number). The results of the experiments show that higher wire numbers, smaller gap spacings produced higher radiated powers and faster rise times. From one-dimensional simulations of single wire explosions using the Desjarlais resistivity model, the high number wires, to first order, merged at least 50 ns before significant acceleration of the array occurred. (This merger has also been observed in preliminary low resolution 2-D r–θ simulations; Douglas *et al*., 2000*c*.) Two dimensional r–z simulations were consistent with this picture—for wire numbers above 56, that is, 2 mm interwire-gap spacing, the simulations could reproduce radiative properties using an initial perturbation level of less than 5%. For wire numbers comparable or lower than this, the 2-D r–z simulations could not adequately model the radiative properties, even with large initial perturbation levels, that is, above 10%. One-dimensional wire simulations show that in the large gap cases, the wires did not merge prior to array acceleration. This critical interwire gap of 2 mm agrees with the scaling one would anticipate from the heuristic model of Haines (1998).

Based on both Imperial College data and combined Saturn experiments and simulations, there appear to be two different regimes for wire array implosions. These regimes are essentially defined by the interwire-gap spacing, the expansion velocity of the wire, and the time it takes for the wire array to acquire a substantial acceleration. Three-dimensional simulations are required for the case where the gap spacing is large enough that merger does not occur for most of the implosion. Two-dimensional r–θ simulations are quite useful in these configurations, but cannot take into account the true 3-D nature of the implosion. Thus, 3-D modeling is required for detailed analysis. For expansion velocities and gap spacings where merger occurs early in the experiment, that is, preferably prior to acceleration, a shell-like implosion is inferred. To date, most simulations of z-pinch implosions have defined the initial condition of the load as a plasma shell, incorporating higher-dimensional effects through the modification of transport coefficients (Thornhill *et al*., 1994) or instability seeding. As noted earlier, such approaches have produced reasonable results for many applications. Recent numerical evidence (M.R. Douglas & C. Deeney, pers. comm.) suggests that for a broadband blackbody source, a shell-like implosion is most desirable. In this case, MRT instabilities dominate the implosion phase of the pinch and the effects of MRT development on pinch performance has a particular meaning and can be modeled. It is this latter configuration that will be addressed in the rest of this paper.

3.1. Conventional 2-D r–z modeling of z pinch implosions

Many types of z pinches are susceptible to MRT instabilities; the strongest experimental evidence of MRT in pinches is from pinhole images of gas puffs, where the load can be observed throughout the implosion phase (Douglas *et al*., 1997; Levine *et al*., 2001; Porter, pers. comm.). As mentioned, past z-pinch simulations have typically used a random-density seed to model perturbation growth. The reason for this is that a random-density formulation has been found to provide good matches with a large range of experiments. For example, Peterson has successfully shown agreement in radiation quantities and physical appearance using a random-density seed for loads on four different experimental machines: Pegasus (Peterson *et al*., 1996), Procyon (explosive generator, Bowers *et al*., 1996), Saturn (Sanford *et al*., 1997), and Z (Peterson *et al*., 1997, 1999; Spielman *et al*., 1998). One such case is illustrated in Figure 1. The Pegasus and Procyon experiments involved thin annular foils, while Saturn and Z involved wire arrays. In addition, Douglas has shown good agreement with Saturn wire-array experiments in the long-pulse mode (Douglas *et al*., 2000*a*) and a variety of tungsten wire experiments on Z (Deeney *et al*., 1999; Douglas *et al*., 2000*b*) in both the short- and long-pulse modes. Roderick *et al*. (1998), Hammer *et al*. (1996), and Douglas *et al*. (1997) have also successfully modeled Saturn gas-puff experiments using this method. It is interesting to note that for a series of Saturn krypton gas-puff experiments (Spielman *et al*., 1994), the observed instability features were numerically simulated based on an initial nozzle injection calculation rather than a random density seed. The nozzle flow calculation produced a density gradient in both the radial and axial directions (expansion fan) which acted as a density seed for the instability. Roderick *et al*. (1998) has shown that a Fourier decomposition of this distribution produces a spectrum composed of a large number of modes of varying amplitudes—a broad mode distribution. It is probable that the initiation of wires in a wire array leads to a similar broad spectrum of modes.

It should be noted that the 2-D r–z wire-array simulations mentioned above have been done for high wire numbers. However, a high wire number wire array may still have significant perturbations in the azimuthal direction, caused by azimuthal asymmetries in the return current path that cannot be modeled in a 2-D r–z code. This concern may be neglected to first order since the stabilizing effect of the azimuthal field in z-pinch configurations suggests that the dominant mode growth is in the r–z plane (Roderick *et al*.,

https://doi.org/10.1017/S0263034600194029 Published online by Cambridge University Press

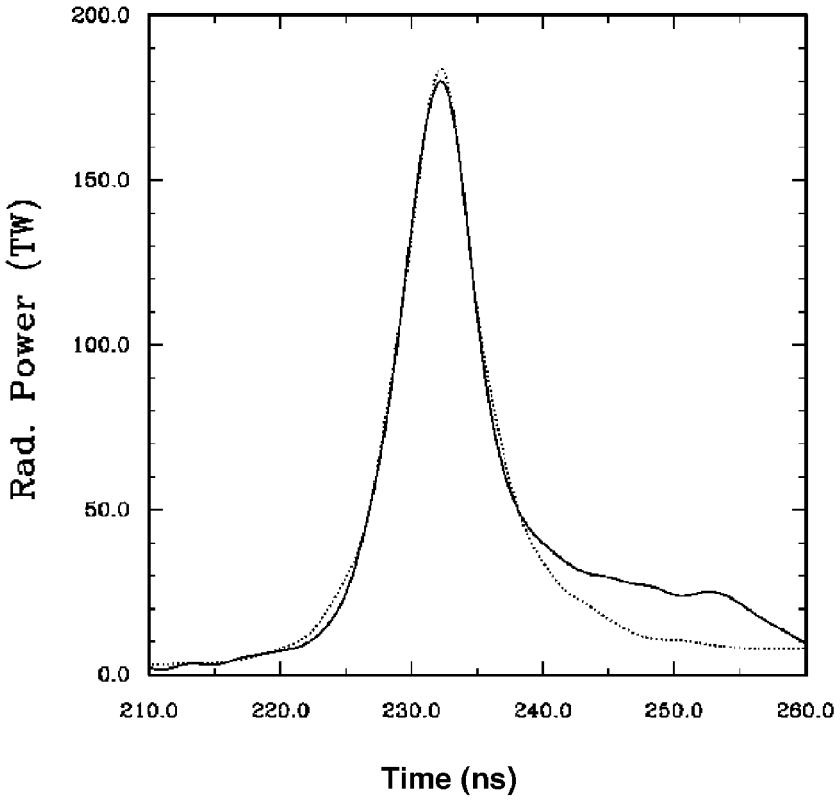

Fig. 1. Overlay of experimentally measured radiated power and the power obtained from a 2-D *r*–*z* simulation for a 4-mg, 240-wire tungsten array at 40-mm diameter, 20-mm length, driven by the 20-MA Z accelerator. The initial plasma conditions used a 1-mm-thick shell with a 2% cell-to-cell random density perturbation. Courtesy of Darrell Peterson, Los Alamos National Laboratory.

1983; Peterson *et al*., 1996). Overall, the success obtained using a random-density seed perturbation for wire arrays suggests that this may not be a bad approximation even with three-dimensional effects and poor characterization of the initial seeding amplitude.

The evolution of a typical *z*-pinch implosion simulation for parameters characteristic of the Z machine is shown in Figure 2. The 2-D radiation MHD code, Mach2 (Peterkin *et al*., 1998) was used to simulate the implosion of a 40-mm-diameter, 1.0-mm-wide annular tungsten shell with a height of 20 mm and a mass of 3.4 mg. The MRT instability was seeded by a 5% cell-to-cell random density perturbation where the spatial resolution was 0.125 mm in the axial direction and 0.2 mm radially. This corresponds to 160 cells axially and 5 cells radially across the initial shell. The load is driven with an equivalent Z voltage profile obtained from the Screamer (Kiefer & Widner, 1985) transmission line circuit code. The peak current from this simulation was approximately 16 MA with the implosion occurring over 100 ns, as measured from the start of the current rise to the maximum value of the radiated power.

From the isodensity contour plots in Figure 2, the MRT evolution to longer wavelengths is clearly observed from 90 ns to 110 ns, and the structure looks qualitatively similar to that observed experimentally at late times in pinhole framing camera images. To illustrate this wavelength evolution in more detail, a Fourier decomposition of the modes is shown in Figure 3. The spectrum was obtained using IDL (IDL Reference Guide, 1992) by performing a fast Fourier transform (FFT) of the radial averaged density for each axial position. The modes are shown in terms of wave number, defined here as $1/\lambda$, where λ is the wavelength in meters. The initial density profile shows a spectrum with larger amplitudes at longer wavelengths. As the shell implodes, the shorter wavelength modes in the initial spectrum rapidly evolve and saturate, and a progressive transition to longer wavelengths is observed. This is seen more easily by drawing an envelope over the peak amplitudes. There is a strong shift in the spectrum towards wavelengths between 1.67 mm and 3.0 mm observed.

The spectral evolution clearly demonstrates the complex nature of an initial random density seed that is defined by zoning, specified amplitude, and boundary conditions. In fact, the large number of modes make it difficult to follow individual mode development and discriminate between the various factors influencing the mode growth, and hence the final structure of the imploding plasma. Nonetheless, this formulation seems to provide a fairly accurate depiction of the MRT character of an imploding *z* pinch.

The MHD-driven aspect of the instability introduces a number of physical phenomenon that do not occur in fluid R-T calculations: magnetic field diffusion into the load, ohmic heating of the perturbed region, and a time-dependent acceleration determined by current delivery to a load with varying inductance. Radiation, cylindrical implosion geometry, and finite-thickness shells, which are important

https://doi.org/10.1017/S0263034600194029 Published online by Cambridge University Press

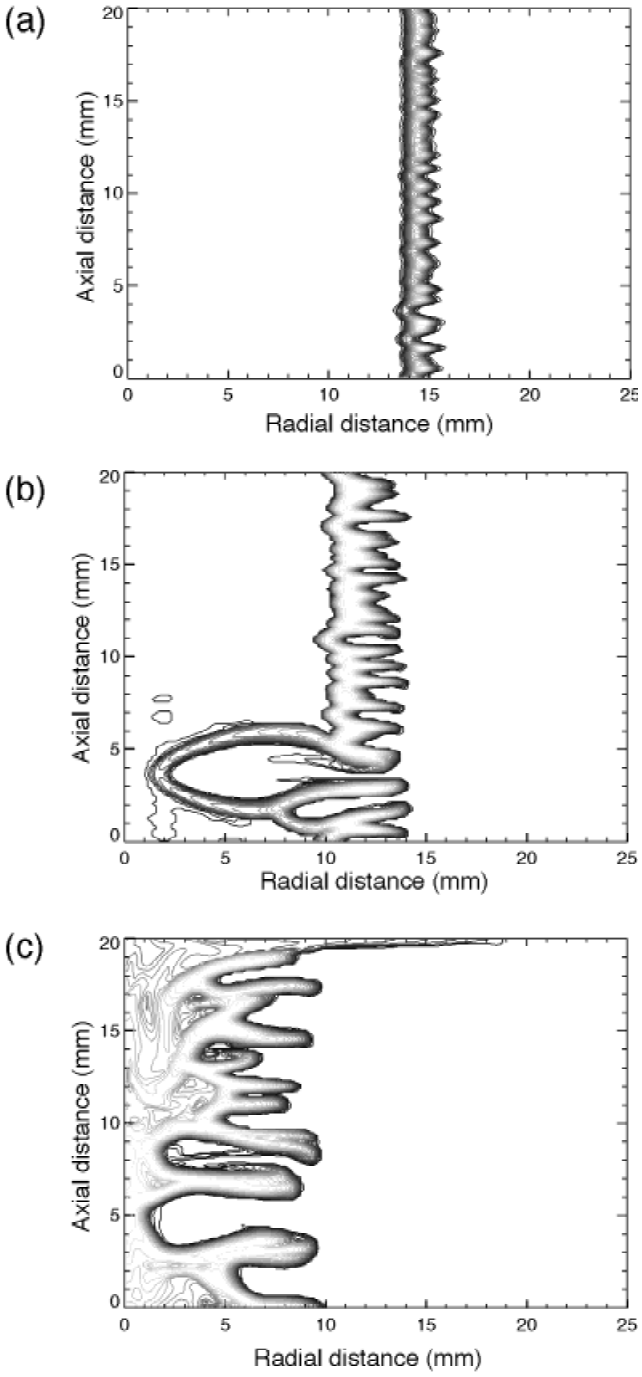

Fig. 2. Evolution of a 40-mm diameter, 20-mm-high, 1-mm-thick annular tungsten load at (a) 90 ns, (b) 100 ns, and (c) 110 ns. The 4.0-mg load was seeded with an initial 5% cell-to-cell random density perturbation.

features in *z*-pinch implosions, further complicate the picture and may dominate the late time behavior of mode development.

To improve our understanding of mode growth and of the physical MHD phenomenon driving the mode development, a recent investigation was carried out that incorporated single-mode and few-mode density profiles (Douglas *et al*., 1998). This approach is similar to that performed by the Inertial Confinement Fusion (ICF) community, where single- and multiple-mode R-T instability growth in both two and three dimensions have been experimentally (Remington *et al*., 1995; Budil *et al*., 1996), computationally (Dahlburg *et al*., 1995; Dunning & Haan, 1995), and theoretically (Haan, 1989, 1991; Hecht *et al*., 1994; Ofer *et al*., 1996) investigated for both ablatively driven and classical (embedded interface) systems. Although single-mode perturbations had previously been used to simulate the MRT instability in gas-puff load design calculations (Cochran *et al*., 1995), there had been no attempt to examine detailed MHD-driven mode development and discrete spectrum effects.

Single-mode calculations not only provide a means to study the qualitative behavior of MRT mode growth, but also the numerical resolution effects on the mode amplitude. Neither issue has been studied extensively in the *z*-pinch community. Two- and three-mode calculations have, in addition, provided a first step in addressing mode-coupling issues that may arise in using a random density seed for standard simulations. Comparison between a random density-seed calculation and that of a single mode of similar amplitude indicate a reduction in mode growth in the former case. Preliminary evidence suggests that this may be the result of mode coupling. A survey of single-mode amplitude versus wavelength revealed that for a given initial perturbation amplitude, the corresponding FFT-spectrum amplitude taken from the calculation significantly decreased for wavelengths that were resolved by less than 10 cells. This effect most likely explains the mode structure observed in simulations with a random density seed, where shorter-wavelength modes exhibit a continual decrease in amplitude until the resolution limit is reached. The effect of resolution was also observed to play a role in mode development during the run-in phase of the implosion. Coarse resolution ($<$20 cells per wavelength) was shown to slow the growth rate of shorter wavelength modes, directly influencing the harmonic growth in most cases. This trend has been observed by others in hydrodynamic simulations and has been considered akin to the stabilizing processes found with viscosity or surface tension.

The early evolution of single-mode growth is qualitatively similar to that seen with hydrodynamic R-T. The single modes grow exponentially in the linear phase and are observed to transition into a nonlinear regime characterized by the appearance of higher harmonics in the FFT spectrum. As the plasma evolves into a bubble-spike structure, the mode growth remains exponential in nature and the modes are not observed to saturate in the classical hydrodynamic sense. This continued exponentiation throughout the latter stages of the implosion is attributed to the finite load thickness. In all cases, the equivalent growth rate, defined by an exponential fit to the time-dependent amplitude spectrum, was much lower than that calculated from linear theory. For the two- and three-mode cases considered, the early time amplitude growth was identical to its single-mode counterpoints. At late times, however, the growth rate of the differ-

https://doi.org/10.1017/S0263034600194029 Published online by Cambridge University Press

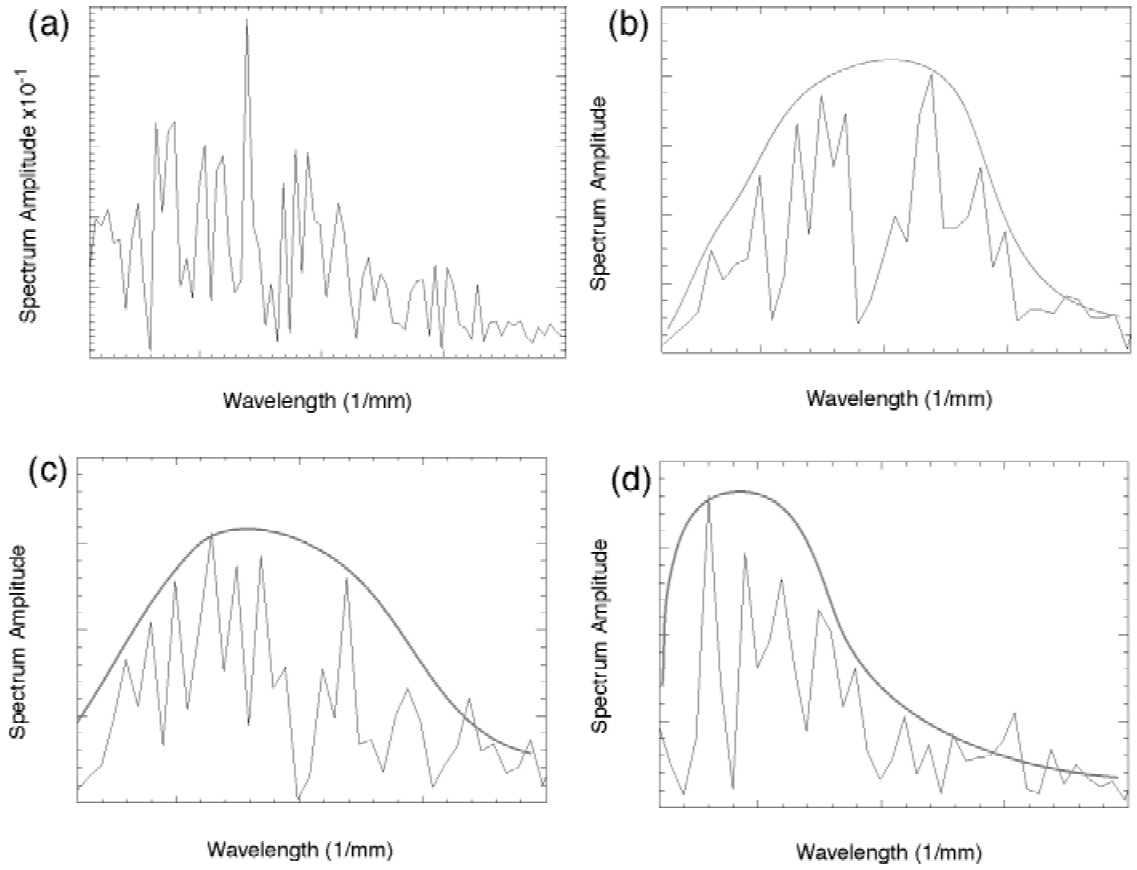

Fig. 3. Spectral evolution of the 1-mm-thick load of Figure 2. The spectrum is obtained by performing an FFT of the (a) initial shell, and the perturbed shell at (b) 90 ns, (c) 100 ns, and (d) 110 ns.

ent components deviated from that of the single-mode cases and a distinct modal variation in the density profile was observed. Both two- and three-mode cases exhibited mode coupling where evidence of both indirect and direct cascade was observed.

As evidenced with this preliminary study, MRT instability growth is complicated, whether single mode, multiple mode, or random-density perturbations are used to seed the instability. Clearly, there are a number of remaining issues that need to be addressed before a comprehensive description of the MRT instability evolution can be determined. Future work should quantify the contributions from radial convergence, magnetic diffusion, finite load thickness, and time-dependent acceleration. Furthermore, an understanding of resolution issues and their effect on mode growth, as well as the influence and sensitivity of the radiation, resistivity, and EOS models should be explored in more detail.

3.2. MRT mitigation schemes—simulations and experiments

For *z*-pinch configurations that are dominated by MRT growth in the implosion phase, pinch performance can be drastically improved by reducing the amplitude of the instability. Some of this can be accomplished through load fabrication and treatment to reduce the initial amplitudes of the unstable modes. This work is in progress and has yet to be understood on a level that can be utilized. In the case of wire arrays, suggestions with regard to wire cleaning, incorporating specific wires based on their explosive properties, and fabricating defined initial perturbations on wires (Ryutov *et al*., 2000) have been made. Some of these suggestions have been examined at a fundamental level, that is, wire cleaning (Mosher *et al*., 1998; Pikuz *et al*., 1999; Cuneo, M.E., pers. comm.) and the results are inconclusive. Others, such as the prescribed perturbations, have yet to be realized.

MRT mode development can also be reduced during the implosion phase via clever design. Many techniques have been suggested to mitigate the MRT growth in such implosions, including uniform-fill loads, that is, uniform-fill gas puffs (Cochran *et al*., 1995), increasing Z (Douglas *et al*., 1996), shear flow (Douglas *et al*., 1997; Shumlak & Roderick, 1998; Velikovich *et al*., 1998), rotation (Velikovich & Davis, 1995), magnetic field stabilization (Bud'ko *et al*., 1990), 3-D azimuthal (ablative) flow (De Groot *et al*.,

https://doi.org/10.1017/S0263034600194029 Published online by Cambridge University Press

2000), and tailored density profiles (Hammer *et al*., 1996; Velikovich *et al*., 1996, 1998). Included in this latter mitigation scheme are multiple shell configurations most easily constructed experimentally as multiple gas puffs or nested wire arrays. Below is a brief summary of the more successful mitigating schemes and associated experimental observations that provided an initial insight or substantiated the design through proof of principle. This is then followed by a brief discussion on viscosity and 3-D effects, both of which are believed to play an important role in MRT mitigation, but are difficult to verify experimentally. Although field stabilization with an axial field has often been proposed and attempted as a mitigating scheme, it has yet to be successfully demonstrated on large current machines (>3 MA) and will not be discussed (see Bud'ko *et al*., 1989, concerning maximum B_z at which magnetic pressure dominates degrading pinch compression).

3.2.1. Uniform fill loads

Experiments have been carried out indicating that uniform-fill gas-puff implosions are more stable to MRT growth than annular implosions (Wong *et al*., 1996; C. Deeney, pers. comm.). Simulations by Roderick *et al*. (1998) with an argon gas puff have shown that uniform-fill gas puffs have less severe bubble-spike structure compared to hollow pinches. This improved stability was also illustrated by Cochran *et al*. (1995) and explained theoretically based on snowplow stabilization (Gol'berg & Velikovich, 1993). An example of this behavior is shown in Figure 4 for a 4.5-cm-diameter uniform and annular (2.5-cm inner diameter) krypton gas puff. The initial gas distribution was approximated by applying a constant-density flow-through boundary condition at the cathode, and allowing the density to reach a steady-state configuration with an open anode. The images in Figure 4a are the resulting density profiles in the two cases. (The centerline, or pinch axis, is at the left boundary.) The total mass was 300 μg for the annular gas puff and 500 μg for the uniform fill. The implosion was driven by a Saturn voltage profile using a self-consistent RL circuit model. The resolution along the pinch axis was 0.2 mm, allowing ~10 cells to resolve 2-mm wave structures.

Isodensity contours prior to stagnation are shown in Figure 4b. Clearly, the solid-fill implosions are more stable, particularly at the inner surface of the sheath region, and the

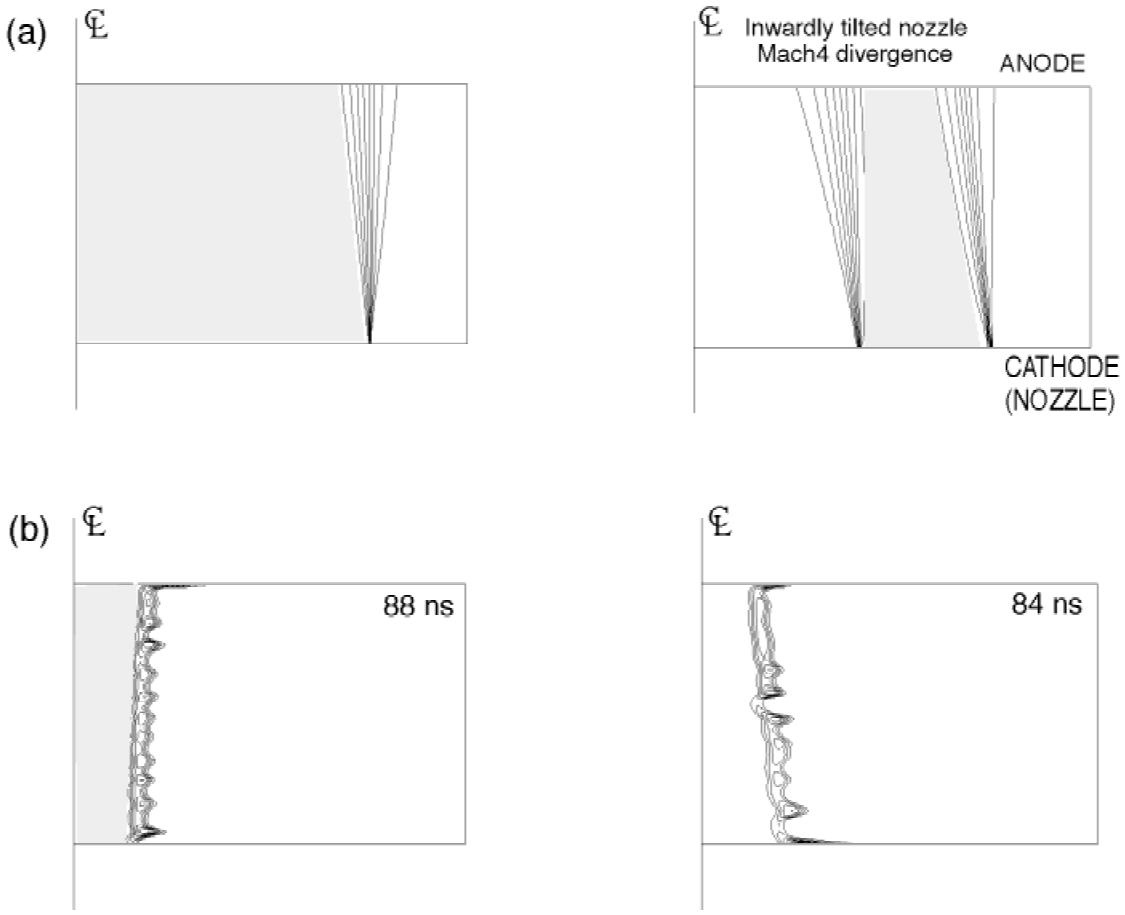

Fig. 4. Isodensity contours for a uniform-fill and annular gas puff (left to right) at (a) initial distribution and (b) late in the implosion.

https://doi.org/10.1017/S0263034600194029 Published online by Cambridge University Press

amplitudes of the modes are smaller. It should be noted that the axial gradient in the initial density profile due to the expansion fan is enough to initiate the instability.

3.2.2. *Higher-Z material*

There is some experimental evidence that suggest an improvement in pinch uniformity with increasing atomic number of the load material. This has been directly observed with uniform-fill gas puffs (Douglas *et al*., 1996) and is suggestive even in wire arrays where pinhole images late in the implosion reveal more uniform behavior in higher-*Z* elements. Past experiments with gas puffs on Saturn have shown reduced MRT growth upon replacing neon with krypton. High-resolution simulations using neon, argon, and krypton 4.5-cm-diameter uniform-fill gas puffs have further illustrated this reduction in MRT growth. The results of these calculations are shown in Figure 5. The injected gas distribution was approximated with a uniform density, right cylinder slab at a radius of 2.25 cm and height of 2.0 cm. To seed the MRT instability, a 5% random cell-to-cell density perturbation was defined throughout the slab, providing the same amplitude and wavelength structure typically observed in experiment. (The slab/perturbation approximation produces near identical results to those with a gradient in *r* and *z*, i.e., the expansion fan, justifying the use of this simple technique.) The total mass in each case was nominally 500 μg.

Density profiles at 95 ns are shown in Figure 5 for the three different working gases. It is apparent that the MRT instability is severely disruptive in the neon case by this time. An increase in the atomic number, however, appears to have a mitigating effect on the MRT growth as evidenced with the argon. There, the sheath region is much broader, and the instabilities are uniformly distributed across the surface with smaller amplitudes. Similar, but less dramatic improvement is seen by replacing argon with krypton.

This observed computational reduction in the MRT instability is related to the current penetration into the plasma. In these calculations, an increase in atomic number leads to a larger number of free electrons (Z) in the sheath region. This in turn, enhances the local plasma resistivity in the sheath:

$$\eta \propto \frac{\bar{Z}}{T_e^{3/2}}.$$

(With each increase in *Z*, the total number of particles decreases approximately by a factor of two, allowing a higher kinetic energy per ion, and hence, a higher ionization at stagnation.) With larger *Z*, the magnetic field can then diffuse further into the plasma (as seen by the extended current sheath), broadening the field diffusion scale length. For the MHD MRT instability, this is known to effectively stabilize the short wavelength growth via magnetic smoothing (Roderick & Hussey, 1986; Hammer *et al*., 1996).

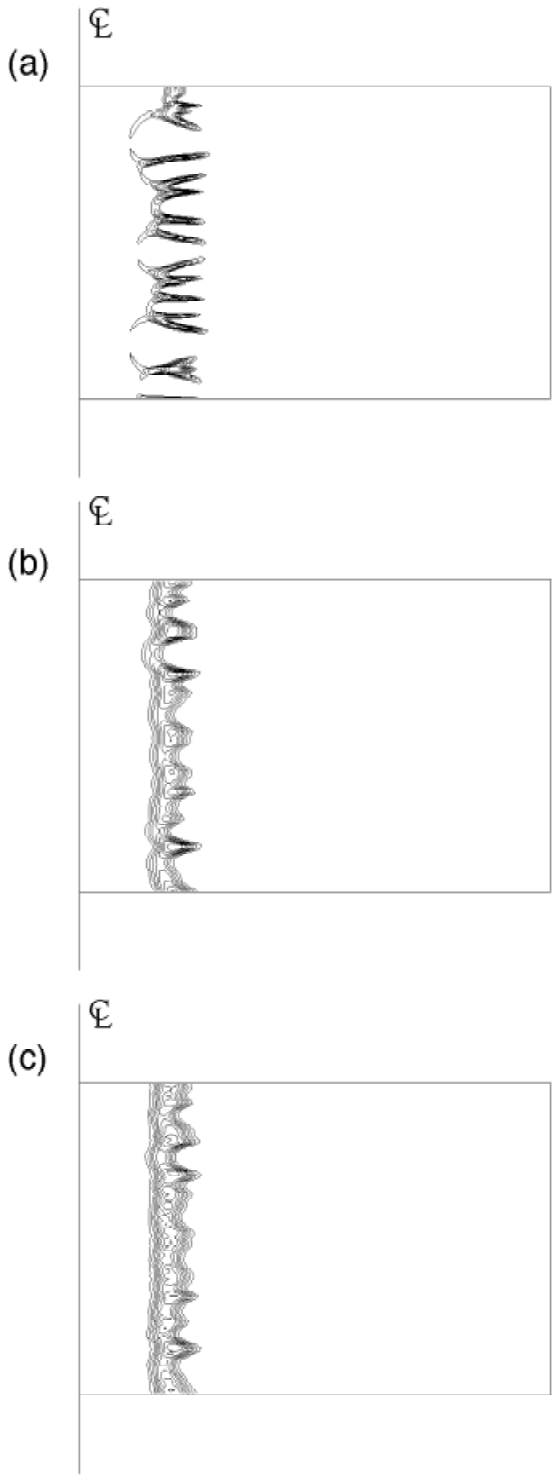

Fig. 5. Isodensity contours at 95 ns into the implosion for a 4.5-cm-diameter uniform fill comprised of (a) neon, (b) argon, and (c) krypton. In each case, the initial load was seeded with a 5% cell-to-cell random density perturbation.

3.2.3. *Shear flow introduced from load curvature*

Camera pinhole images of the neon/krypton gas-puff experiments mentioned above also exhibited a unique feature in the uniform-fill cases. In these particular experiments, a

https://doi.org/10.1017/S0263034600194029 Published online by Cambridge University Press

curved sheath at the plasma–vacuum interface was seen during the observable portion of the implosion phase. This "hourglassing" configuration was attributed to the divergence of the gas flow coupled with an axial mass gradient. [Similar to the long-wavelength effects that produce zippering (Pereira & Davis, 1988) in gas puffs.] Experimental data showed that the hourglassing was fairly severe and was maintained throughout the implosion. In addition, the amount of MRT structure appeared minimal, suggesting that the curvature may have an effect on MRT development.

Simulations by Douglas *et al*. (1997) show that the experimentally observed MRT reduction also occurs in the modeling. (Calculations ranged from a uniform slab with a flat outer surface to a concave surface with increasing degrees of curvature; a random density perturbation was used to seed the instability.) The simulations indicate that the MRT reduction is caused by material flow along the curved plasma surface, convecting the instabilities toward the computational wall boundaries. Such mass flow with curved sheaths has also been demonstrated in plasma focus geometries (Potter, 1971). Computational diagnostics that measure the shear velocity flow along the curved surfaces suggests axial velocities on the order of 10% or more of the radial velocity are needed to slow MRT growth. This value is similar to that obtained by Shumlak and Roderick (1998) and in work concerning flow stabilization of the kink instability (Shumlak & Hartman, 1995; Arber & Howel, 1996).

The effects of curvature on MRT development is illustrated in Figure 6. Simulations were carried out on a 4.0-cm-diameter load comprised of argon with varying degrees of outer surface curvature. Shown in the figure are isodensity contour profiles at 90 ns into the implosion for (a) an initially flat surface, and (b) an initially curved surface defined by a 2.5-mm circular arc. The top and bottom electrodes are defined as perfectly conducting walls. The mitigating effect on MRT is clearly demonstrated.

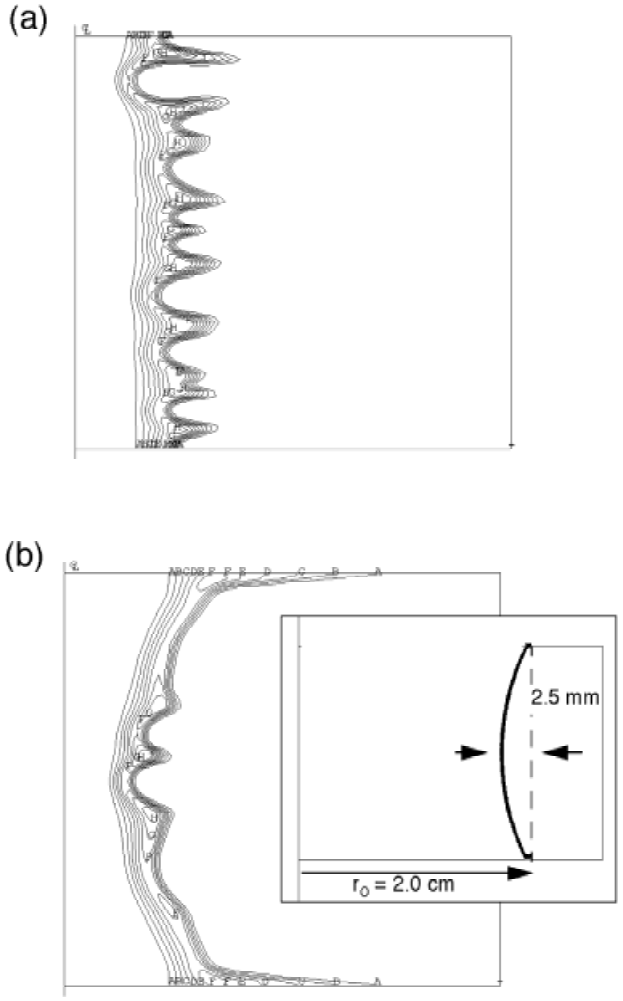

Fig. 6. Isodensity contour plots illustrating the effect of sheath curvature on a 4-cm-diameter uniform argon gas puff prior to stagnation: (a) initially uniform surface and (b) initially imposed 2.5-mm arc.

3.2.4. Tailored density profiles—nested configurations

As observed both experimentally and computationally, uniform-fill gas puffs exhibit a higher degree of uniformity and symmetry compared to annular gas-puff distributions (Sec. 3.1). This is primarily due to a reduction in the MRT development as seen in subkiloelectron volt X-ray pinhole camera images of the implosion. In the case of the uniform fill, mitigation of the magnetically driven MRT growth is believed to occur through mass accretion and shocked-region back pressure (Gol'berg & Velikovich, 1993) as the unstable interface encounters downstream material. Although this mitigation scheme greatly improves pinch uniformity, the load itself couples less efficiently with the pulsed-power machine and a lower total X-ray energy is measured compared to its annular counterpart.

This apparent trade-off between pinch stability and energy coupling has been examined with a series of 2-D MHD simulations (Douglas *et al*., 2001) and is illustrated in Figure 7. In the simulations, a 4.0-cm-diameter, 2.0-cm-high, 3.4-mg aluminum load, which varied in thickness from a 1-mm shell to a completely filled cylinder, was driven by the same voltage waveform. To model the instability, a 5% cell-to-cell random density seed was incorporated into the initial density profile. The peak (mass-averaged) radial velocity, which is a measure of the energy coupling to the load, is plotted as a function of shell thickness. Also plotted are the velocities for the corresponding unseeded (one-dimensional) implosions. From the figure, it is clear that the thinner shells provide the largest velocities, and hence, improved energy coupling, as long as the MRT instability is absent. When the instability is present, the uniform-fill simulations are least affected, as seen by the minor decline in radial velocity. The thinnest shells, on the other hand, deviate substantially from the 1-D case; late in the implosion they become severely distorted, leading to lower final velocities, lower temperatures, and broader radiation pulses. The final velocities achieved for these unstable thin shells are equivalent to those of the uniform-fill loads. Such results suggest that the

https://doi.org/10.1017/S0263034600194029 Published online by Cambridge University Press

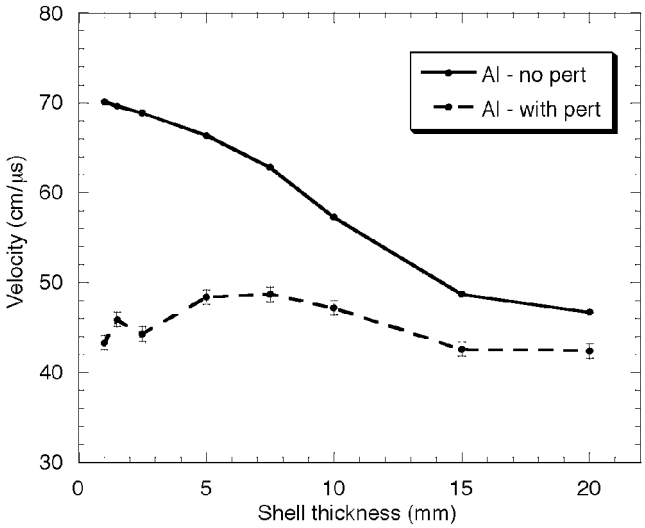

Fig. 7. Peak radial velocity as a function of load thickness for aluminum pinch characteristic of that imploded on the Z accelerator. The solid curve shows the results for an initially unperturbed aluminum implosion. The other curve illustrates the trend observed when an initial 5% cell-to-cell random density seed is incorporated into the initial conditions.

optimal mitigation scheme, which maximizes both pinch uniformity and efficient energy coupling for a specific application, may be somewhere in between the two extremes of a thin shell or a uniform fill.

One approach in minimizing the MRT growth while still maintaining the optimal energy coupling that comes with a thin shell is to insert an additional shell downstream of the original load. Computationally the shell would be placed at a position to minimize the MRT development; intuitively one might consider this location to be defined by the observed onset of nonlinear MRT growth. The combined influence of mass accretion (see Book, 1996, for discussion of nonlinear R-T reduction via mass accretion utilizing multiple shells) and deceleration from this "tuning layer" would then slow or even reverse the growth of the MRT instability. This type of design is amenable to gas puffs, since they behave much like annular shells. Indeed, MRT mitigation has been directly observed (via pinhole images) and inferred (from increases in *K*-shell type emissions suggesting high pinch compression ratios) from double shell (Baksht *et al*., 1995, 1996; Shishlov *et al*., 2000; Sze *et al*., 2000) and multiple-shell gas puffs (Luchinsky, 1993). Another related technique involves tailored density profiles that introduce a mass distribution that maintains a near zero-to-zero acceleration (Hammer *et al*., 1996; Velikovich *et al*., 1996, 1997) of the imploding shell. Such configurations have yet to be experimentally demonstrated.

With mass accretion alone, one can envision that a minimum density exists below which the accretion rate is insufficient to impede the MRT development. This minimum required "floor" density can be determined to zero order by equating the force due to accrued mass (back pressure) at the bubble surface and the $\mathbf{J} \times \mathbf{B}$ accelerating force. For a right circular cylinder of height l, the mass that is swept up over a distance Δr of the implosion is given by $\rho(2\pi r \Delta r l)$. The rate of accretion is then

$$\dot{m} = \frac{m_{(\Delta r)}}{\Delta t} = \frac{m_{(\Delta r)}}{\Delta r} v = 2\pi\rho v l,$$

where v is the instantaneous implosion velocity. To slow bubble penetration into the load, the change in momentum, $\dot{m}v$, at the plasma-bubble interface should be on the order of the accelerating force. Approximating this by

$$\frac{\mu_0 I^2}{4\pi r} l$$

an estimate for this floor density can be found:

$$\rho_{floor} = \frac{\mu_0 I}{8\pi^2 r^2 v^2}.$$

Combining this estimate with experience based on double gas puffs, designs can be developed computationally to improve the performance of any annular pinch configuration. This approach has even been used successfully with high wire number tungsten arrays on the Z accelerator. In particular, an approximately 40% improvement in peak radiated power has been experimentally observed by placing a tungsten array inside that of a standard 4-mg, 40-mm-diameter array (Deeney *et al*., 1998). Based on numerical simulations, the inner array was placed at 20 mm, with $\frac{1}{2}$ the mass of the outer array. Although the 2-D MHD simulation predicted a much higher power than that measured (340 TW compared to 280 ± 40 TW), the qualitative trend was experimentally demonstrated—compelling evidence that such configurations can work.

3.2.5. Viscosity

Viscosity may be an additional factor in reducing MRT growth observed in uniform-fill gas puffs. In a nonmagnetized viscous fluid, it has been shown that the growth rate of the R-T instability is reduced (Chandrasekhar, 1961). The effect of viscosity on the MRT instability is more complicated. As shown by Ryutov *et al*. (2000), the effect of viscosity is dependent on the ratio of ion–ion mean-free-path, λ_{ii}, to the scale height of the density gradient, h, that is, $R = \lambda_{ii}/h$. The ion density is high and the ion temperature is low in typical wire array plasmas, so the ratio R is much less than one and the effect of viscosity is negligible. However, for large diameter gas puff loads (De Groot *et al*., 1997*a*,*b*) the ratio R can be of order 1, and viscosity can reduce the growth rate of the MRT instability.

3.2.6. Three-dimensional effects—azimuthal flow

Wire arrays are resistively heated and turned into individual plasmas with an azimuthal periodicity equal to the initial number of wires. The resultant shell has density peaks at the

https://doi.org/10.1017/S0263034600194029 Published online by Cambridge University Press

initial position of the wires and density valleys between the initial wire positions. As the number of wires is increased, the difference between the densities of the peak and valley decrease. For a very large number of wires, the shell approaches complete azimuthal symmetry. The MRT instability for the plasma produced by a finite number of wires is quite different as compared to a completely symmetric shell. In the former case, when the individual plasmas are perturbed in the axial direction, the plasma can move in the azimuthal direction and smooth the perturbation (De Groot *et al*., 2000). This effect could reduce the MRT instability growth rate. Three-dimensional MHD calculations are now under way to evaluate the importance of this effect.

4. SUMMARY

The MRT instability is believed to be the dominant effect in degrading the performance of many, but not all, dynamic *z* pinches. This is particularly true for gas puffs, foils, and high wire number arrays. The amplitude of the MRT instability can be decreased by reducing the initial amplitude of the unstable modes and/or reducing the growth rate of the instability. Careful design of the *z*-pinch load can reduce both of these effects. To this end, approaches in MRT mitigation have been developed and experimentally verified. Two-dimensional MHD calculations (both r–z and r–θ) have matured to the point where quite good agreement between simulations and experiments have been obtained, especially in the case of a very large number of wires in a wire array. The calculations have increased our understanding of dynamic *z* pinches and have guided some experiments that have resulted in enhancing the pinch performance.

REFERENCES

Arber, T.D. & Howell, D.F. (1996). *Phys. Plasmas* **3**, 544.
Baksht, R.B. *et al.* (1995). *Plasma Phys. Reports* **21**, 907.
Baksht, R.B. *et al.* (1996). *Plasma Phys. Reports* **22**, 563.
Beg, F.N. *et al.* (1997). *Plasma Phys. Controlled Fusion* **39**, 1.
Book, D.L. (1996). *Phys. Plasmas* **3**, 354.
Budil, K.S. *et al*. (1996). *Phys. Rev. Lett.* **76**, 4536.
Bud'ko, A.B. *et al.* (1989). *Phys. Fluids B* **1**, 598.
Bud'ko, A.B. *et al.* (1990). *Phys. Fluids B* **2**, 1159.
Bowers, R.L. *et al*. (1996). *Phys. Plasmas* **3**, 3448.
Chandrasekhar, S. (1961). *Hydrodynamic and Hydromagnetic Stability* Oxford: Clarendon.
Chittenden, J.P. *et al.* (1997). *Phys. Plasmas* **4**, 4309.
Chittenden, J.P. *et al.* (1999). *Phys. Rev. Lett.* **83**, 100.
Chittenden, J.P. *et al.* (2000). *Phys. Rev. E* **61**, 4370.
Chittenden, J.P. *et al.* (2001). *Laser Part. Beams* **19**, xxx.
Cochran, F.L. *et al*. (1995). *Phys. Plasmas* **2**, 1.
Dahlburg, J.P. *et al*. (1993). *Phys. Fluids B* **5**, 571.
Dahlburg, J.P. *et al*. (1995). *Phys. Plasmas* **2**, 2453.
Deeney, C. *et al*. (1993). *Phys. Fluids B* **5**, 992.
Deeney, C. *et al*. (1997*a*). *Phys. Rev. E* **56**, 5945.
Deeney, C. *et al*. (1997*b*). *Rev. Sci. Instrum*. **68**, 653.
Deeney, C. *et al*. (1998). *Phys. Rev. Lett.* **81**, 4883.
Deeney, C. *et al.* (1999). *Phys. Plasmas* **6**, 3576.
Deeney, C. *et al.* (2000). *Bull. Am. Phys. Soc*. **45**, 139.
De Groot, J.S. *et al*. (1997*a*). *Phys. Plasmas* **4**, 737.
De Groot, J.S. *et al.* (1997*b*). In *Proc. Fourth Int. Conf. on Dense Z Pinches* (Pereira, N.R., Davis, J., and Pulsifer, P.E., Eds.), AIP Conference Proc., Vol. 409, p.157. Woodbury, NY: AIP.
De Groot, J. S. *et al*. (2000). In *Proc. 2nd Annual Workshop on the Physics of Wire-Array Z-Pinch Plasmas*, Taos NM.
Desjarlais, M.P. (2001). *Contrib. Plasma. Phys.* **41**, 267.
Desjarlais, M.P. & Marder, B.M. (1999*a*). *Phys. Plasmas* **6**, 2057.
Desjarlais, M.P. *et al*. (1999*b*). *Bull. Am. Phys. Soc.* **45**, 141.
Derzon, M.S. *et al.* (1997). *Rev. Sci. Instrum.* **68**, 848.
Douglas, M.R. *et al.* (1996). *Bull. Am. Phys. Soc.* **41**, 1469.
Douglas, M.R. *et al*. (1997). *Phys. Rev. Lett.* **78**, 4577.
Douglas, M.R. *et al*. (1998). *Phys. Plasmas* **5**, 4183.
Douglas, M.R. *et al.* (2000*a*). *Phys. Plasmas* **7**, 2945.
Douglas, M.R. *et al*. (2000*b*). *Phys. Plasmas* **7**, 1935.
Douglas, M.R. *et al.* (2000*c*). *Bull. Am. Phys. Soc.* **45**, 140.
Douglas, M.R. *et al*. (2001). *Phys. Plasmas* **8**, 238.
Dunning, M.J. & Haan, S.W. (1995). *Phys. Plasmas* **2**, 1669.
Figura, E.S. *et al*. (1991). *Phys. Fluids B* **3**, 2835.
Giuliani, J.L., Jr. *et al*. (1990). *J. Quant. Spectros. Radiat. Transfer* **44**, 471.
Gol'berg, S.M. & Velikovich, A.L. (1993). *Phys. Fluids B* **5**, 1164.
Haan, S.W. (1989). *Phys. Rev. A* **39**, 5812.
Haan, S.W. (1991). *Phys. Fluids B* **3**, 2349.
Haines, M.G. (1998). *IEEE Trans. Plasma Sci.* **26**, 1275.
Hammer, J.H. & Ryutov, D.D. (1999). *Phys. Plasmas* **6**, 3302.
Hammer, J.H. *et al*. (1996). *Phys. Plasmas* **3**, 2063.
Hecht, J. *et al*. (1994). *Phys. Fluids* **6**, 4019.
Hussey, T.W. & Roderick, N.F. (1981). *Phys. Fluids* **24**, 1384.
Hussey, T.W. *et al*. (1980). *J. Appl. Phys.* **51**, 1462.
Hussey, T.W. *et al.* (1986). *J. Appl. Phys.* **58**, 2677.
Hussey, T.W. *et al.* (1995). *Phys. Plasmas* **2**, 2055.
IDL Reference Guide (1992). Boulder, CO: Research Systems, Inc.
Kiefer, M.L. & Widner, M.M. (1985). *Digest of Tech. Papers, Fifth IEEE Pulsed Power Conf.* (Rose, M.F. and Turchi, P.J., Eds.), p. 685. Piscataway, NJ: Institute of Electrical and Electronic Engineers.
Kloc, D.A. *et al*. (1982). *J. Appl. Phys.* **53**, 6706.
Kull, H.J. (1991). *Physics Reports* **206**, 197.
Lebedev, S.V. *et al.* (1998). *Phys. Rev. Lett.* **81**, 4152.
Lebedev, S.V. *et al*. (1999). *Phys. Plasmas* **6**, 2016.
Lebedev, S.V. *et al*. (2000). *Phys. Rev. Lett.* **85**, 98.
Levine, J.S. *et al.* (2001). *Phys. Plasmas* **8**, 533.
Liberman, M.A. *et al.* (1999). *Physics of High-Density Z-Pinch Plasmas*. New York: Springer-Verlag.
Lindl, J. (1995). *Phys. Plasmas* **2**, 3933.
Manheimer, W. *et al*. (1984). *Phys. Fluids* **27**, 2164.
Matuska, W. *et al*. (1996). *Phys. Plasmas* **3**, 1415.
Mitchell, I.H. *et al.* (1996). *Rev. Sci. Instrum.* **67**, 1533.
Mosher, D. *et al*. (1998). *Bull. Am. Phys. Soc*. **43**, 1642
Ofer, D. *et al*. (1996). *Phys. Plasmas* **3**, 3073.
Orszag, S.A. (1984). *Physica D* **12**, 19.
Pereira, N.R. & Davis, J. (1988). *J. Appl. Phys.* **64**, R3.
Peterkin, R.E., Jr. *et al*. (1998). *J. Comp. Phys.* **140**, 148.
Peterson, D.L. *et al*. (1996). *Phys. Plasmas* **3**, 368.
Peterson, D.L. *et al*. (1997). In *Proc. Fourth Int. Conf. on Dense Z-Pinches* (Pereira, N.R., Davis, J., and Pulsifer, P.F., Eds.), AIP Conf. Proc., Vol. 409, p. 201. Woodbury, NY: AIP.

https://doi.org/10.1017/S0263034600194029 Published online by Cambridge University Press

Peterson, D.L. *et al.* (1999). *Phys. Plasmas* **6**, 2178.
Pikuz, S.A. *et al.* (1999*a*). *Phys. Rev. Lett.* **83**, 4313.
Pikuz, S.A. *et al*. (1999*b*). *Phys. Plasmas* **6**, 4272.
Potter, D.E. (1971). *Phys. Fluids* **14**, 1911.
Reisman, D.B. *et al.* (2001). *Laser Part. Beams* **19**, xxx.
Remington, B.A. *et al.* (1995). *Phys. Plasmas* **2**, 241.
Roderick, N.F. & Hussey, T.W. (1984). *J. Appl. Phys.* **56**, 1387.
Roderick, N.F. & Hussey, T.W. (1986). *J. Appl. Phys.* **59**, 662.
Roderick, N.F. *et al*. (1980). *Appl. Phys. Lett.* **35**, 273.
Roderick, N.F. *et al*. (1983). *Lasers Part. Beams* **1**, 181.
Roderick, N.F. *et al*. (1998). *Phys. Plasmas* **5**, 1477.
Rosenthal, S.E. *et al*. (2000). *IEEE Trans. Plasma Sci.* **28**, 1427.
Ruiz-Camacho, J. *et al*. (1999). *Phys. Plasmas* **6**, 2579.
Ryutov, D.D. *et al*. (2000). *Rev. Mod. Phys.* **72**, 167.
Sakagami, H. & Nishihara, K. (1990). *Phys. Fluids B* **2**, 2715.
Sanford, T.W.L. *et al*. (1996). *Phys. Rev. Lett.* **77**, 5063.
Sanford, T.W.L. *et al*. (1997*a*). In *Proc. Fourth Int. Conf. on Dense Z-Pinches* (Pereira, N.R., Davis, J., and Pulsifer, P.F., Eds.), AIP Conf. Proc., Vol. 409, p. 561. Woodbury, NY: AIP.
Sanford, T.W.L. *et al*. (1997*b*). *Phys. Plasmas* **4**, 2188.
Sanford, T.W.L. *et al.* (1998). *Phys. Plasmas* **5**, 3737.
Sanford, T.W.L. *et al*. (1999). *Phys. Plasmas* **6**, 1270.
Sarkisov, G.S. *et al*. (2001). *JETP Lett.* **2**, 69.
Sharp, D.H. (1984). *Physica D* **12**, 3.
Shelkovenko, T.A. *et al*. (1999). *Rev. Sci. Instrum.* **70**, 667.
Shishlov, A.V. *et al.* (2000). *Phys. Plasmas* **7**, 1252.
Shumlak, U. & Hartman, C.W. (1995). *Phys. Rev. Lett.* **75**, 3285.
Shumlak, U. & Roderick, N.F. (1998). *Phys. Plasmas* **5**, 2384.
Sinars, D.B. *et al*. (2000). *Phys. Plasmas* **7**, 1555.
Sinars, D.B. *et al*. (2001). *Phys. Plasmas* **8**, 216.
Song, Y. *et al.* (2000). *Rev. Sci. Instrum.* **71**, 3080.
Spielman, R.B. *et al.* (1985). *J. Appl. Phys.* **57**, 830.
Spielman, R.B. *et al*. (1989). In *Proc. Second Int. Conf. on Dense Z Pinches* (Pereira, N.R., Davis, J. and Rostoker, N., Eds.), AIP Conf. Proc., Vol. 409, p. 3. Woodbury, NY: AIP.
Spielman, R.B. *et al.* (1998). *Phys. Plasmas* **5**, 2105.
Spielman, R.B. *et al*. (1994). *IEEE Int. Conf. on Plasma Sci.*, p. 161. Piscataway, NJ: Institute of Electrical and Electronic Engineers.
Sze, H. *et al*. (2000). *Phys. Plasmas* **7**, 4223.
Thornhill, J.W. *et al.* (1994). *Phys. Plasmas* **1**, 321.
Town, R.P. & Bell, A.R. (1991). *Phys. Rev. Lett.* **67**, 1863.
Velikovich, A.L. & Davis, J. (1995). *Phys. Plasmas* **2**, 4513.
Velikovich, A.L. *et al*. (1996). *Phys. Rev. Lett.* **77**, 853.
Velikovich, A.L. *et al*. (1997). In *Proc. Fourth Int. Conf. on Dense Z-Pinches* (Pereira, N.R., Davis, J., and Pulsifer, P.F., Eds.), AIP Conf. Proc., Vol. 409, p. 549. Woodbury, NY: AIP.
Velikovich, A.L. *et al.* (1998). *Phys. Plasmas* **5**, 3377.
Wong, K.L. *et al.* (1996). *Bull. Am. Phys. Soc.* **40**, 1859.

https://doi.org/10.1017/S0263034600194029 Published online by Cambridge University Press